Biomacromolecules

pubs.acs.org/Biomac

Article

3D-Printing of Structure-Controlled Antigen Nanoparticles for Vaccine Delivery

Akihiro Nishiguchi, Fumiaki Shima, Smriti Singh, Mitsuru Akashi, and Martin Moeller*

Cite This: *Biomacromolecules* 2020, 21, 2043–2048

Read Online

ACCESS | Metrics & More | Article Recommendations | Supporting Information

ABSTRACT: Targeted delivery of antigens to immune cells using micro/nanocarriers may serve as a therapeutic application for vaccination. However, synthetic carriers have potential drawbacks including cytotoxicity, low encapsulation efficiency of antigen, and lack of a morphological design, which limit the translation of the delivery system to clinical use. Here, we report a carrier-free and three-dimensional (3D)-shape-designed antigen nanoparticle by multiphoton lithography-based 3D-printing. This simple, versatile 3D-printing approach provides freedom for the precise design of particle shapes with a nanoscale resolution. Importantly, shape-designed antigen nanoparticles with distinct aspect ratios show shape-dependent immune responses. The 3D-printing approach for the rational design of nanomaterials with increasing safety, complexity, and efficacy offers an emerging platform to develop vaccine delivery systems and mechanistic understanding.

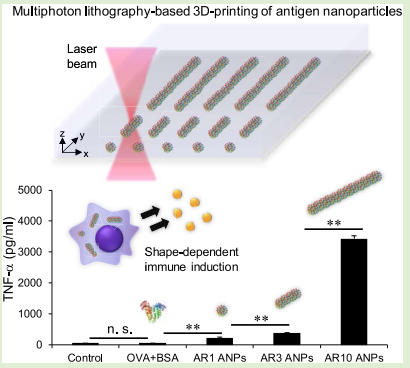

INTRODUCTION

Vaccine delivery aims to manipulate immune responses by targeted delivery of an antigen using micro/nanometer-sized carriers to immune cells for protection and/or treatment against infectious diseases and cancers.[1−3] When antigens such as recombinant proteins and synthetic peptides are taken up by antigen-presenting cells (APCs), they are processed and presented on the APCs, which activates naïve T cells and induces antigen-specific immune responses.[4,5] For immunomanipulation, micro/nanometer-sized polymeric carriers including biodegradable particles,[6,7] micelles,[8] and microgels[9] have been investigated due to their abilities of biodegradability, encapsulation of antigens, targeting by ligands, enhanced uptake by APCs, long-term circulation, and control of the release kinetics. These micro/nanotechnologies may offer an efficient delivery system that provides high therapeutic efficacy and minimizes adverse side effects, thus serving as a safe carrier.[10] Despite considerable efforts, these materials suffer from potential drawbacks including the lack of biocompatibility due to the use of nonbiodegradable, toxic materials like synthetic surfactants or polymers and the low encapsulation efficiency of antigens, which limits the translation of the delivery system to clinical use. The ideal vaccine delivery system should deliver antigens to APCs without using any material apart from the antigen for initiating immune responses.

Antigen particles have attracted much attention as an emerging carrier that does not require carrier materials, and the antigen itself acts as a carrier.[11−15] Assembling of proteins through hydrophobic or electrostatic interactions,[11,12] molding,[13] spray-freeze-drying,[14] and chemical cross-linking[15] form protein particles ranging from hundreds of nanometers to tens of micrometers in size, which might provide safe and efficient vaccination without the use of additional synthetic materials. However, these methods have problems in stability, polydispersity, versatility, and biocompatibility. Moreover, none of them allows for the geometric design and control of particle geometry, although physical properties including size, mechanical strength, topology, and compartmentalization play a major role along with chemical properties.[16−18] In nature, bacteria and viruses display a variety of morphologies, and this diversity of shapes highlights the significance of physical properties in functions for their survival or infection to the host.[16] Along with these, it is also known that particle shape influences the interaction with the cell membrane,[19] phagocytic internalization,[20] and circulation in the blood,[21] which indicates that the geometric design and control of particle shape regulate the immune response. Despite these early studies, there is little mechanistic understanding of the effects of particle shape on immune response due to the limitation of fabrication methods for micro/nanoparticles, especially for those composed of proteins. Therefore, a novel approach to rationally design monodisperse, biocompatible antigen particles is required.

Received: December 25, 2019
Revised: March 8, 2020
Published: April 2, 2020

https://dx.doi.org/10.1021/acs.biomac.9b01775
Biomacromolecules 2020, 21, 2043−2048

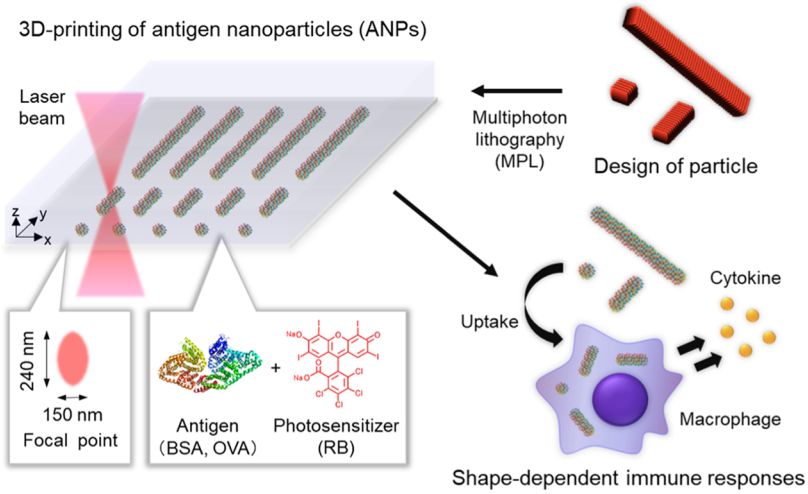

Figure 1. Schematic illustration of the 3D-printing system of ANPs. According to the particle design, a photoresist composed of an antigen and a photosensitizer was used to fabricate shape-defined ANPs by the MPL-based 3D-printing system. The resolution of this system depends on the size of the focal points. The ANPs were taken up by APCs (macrophage) and triggered adaptive immune responses depending on particle shape.

Here, we report a three-dimensional (3D)-printing approach to fabricate carrier-free, shape-controlled antigen nanoparticles (ANPs) (Figure 1). The 3D structures of ANPs were designed with a computer-aided design (CAD) system, and ANPs were prepared using multiphoton lithography (MPL).[22,23] MPL is one of the most powerful 3D-printing platforms to achieve 3D-micro/nanofabrication at high spatial resolution due to the nonlinearity of the optical process (~200 nm). Through the two-photon excitation of a photosensitizer and radical production on the amino acids in antigens,[24,25] antigens were chemically cross-linked to form shape-designed ANPs. The MPL-based 3D-printing approach allows for the fabrication of ANP features on a nanometer scale because the cross-linking reaction is confined to the focal laser volume. We addressed the preparation of ANPs using MPL and tunability of particle shape. Furthermore, shape-dependent immune responses of 3D-printed ANPs with distinct aspect ratios (ARs) were evaluated.

MATERIALS AND METHODS

3D-Printing of ANPs. Protein photoresists for ANPs were prepared by dissolving 40 wt % proteins and 5 mM photosensitizer, rose bengal (RB, Sigma-Aldrich), in phosphate-buffered saline (PBS, pH = 7.4) at 37 °C. Three types of proteins were employed: bovine serum albumin (BSA, M_w = 67 kDa, Sigma-Aldrich), ovalbumin (OVA, albumin from chicken egg, M_w = 10 kDa, Sigma-Aldrich), and gelatin (M_w = 10 kDa, Sigma-Aldrich). Protein photoresists were stored at 4 °C up to 1 week. Before use for MPL, the prepared photoresist was filtrated with a 0.2 μm syringe filter (Whatman). To avoid drying of the photoresist, the photoresist was placed on a coverslip (30 mm in diameter, 0.13−0.16 mm in thickness) with a chamber of poly(dimethylsiloxane) (PDMS; outer dimension of 15 × 15 mm^2 and inner dimension of 10 × 10 mm^2) and covered with a 15 × 15 mm^2 coverslip. The MPL process was performed using the Photonic Professional DLW system (Nanoscribe GmbH, Germany) with an oil-immersion 63× objective lens (numerical aperture (NA): 1.4, Zeiss, Germany). A femtosecond laser (emission wavelength: 780 nm, pulse width: 120 fs, and repetition rate: 100 MHz) was used as a laser source. The structures were designed using CAD software (AutoCAD, Autodesk, CA), and the virus-like structure models were designed using CAD based on the models from NIH 3D Print Exchange. A laser power of 50 mW and a scanning speed of 2000 μm/s were used for MPL of ANPs. ANPs were printed in the solution 10 μm away from a glass substrate to prevent sticking on the glass. The MPL process was carried out for 24 h, and then, the protein photoresist was collected from a chamber by pipetting. The obtained ANPs were purified by dialysis in PBS (pH = 7.4) using a dialysis membrane with a 100 kDa molecular weight cutoff (Spectrum Labs) to remove unreacted proteins and photosensitizer. After 3 days of dialysis, the solution was freeze-dried to obtain ca. 5 mg of ANPs. ANPs were reconstituted with ultrapure water since these contained the salts from PBS.

Characterization of ANPs. The reconstituted ANPs were observed by a confocal laser scanning microscope (CLSM, Leica TCS SPE, Leica, Germany). Since the photosensitizer was conjugated to ANPs through a radical reaction, ANPs could be observed by a fluorescence microscope (excitation wavelength of RB: ~550 nm). ANPs were placed on a coverslip and observed by an oil-immersion 63× objective lens (NA: 1.4, Leica, Germany). The obtained images by a CLSM or an optical microscope were analyzed using Leica Application Suite AF Lite (Leica, Germany) or ImageJ. Scanning electron microscopy (SEM) was performed with an S-4800 ultrahigh-resolution SEM (HITACHI, Japan). Samples were coated with gold, 6 nm in thickness, by spattering for the observation. The accelerating voltage and working distance were set to 10 kV and 10−15 mm, respectively. The size distributions of ANPs in PBS were measured by a dynamic light scattering (DLS) method using a Zetasizer Nano ZS (Malvern Instruments, U.K.).

Cell Culture. The murine macrophage-like cell line RAW264.7 (ECACC, England) was cultured in Dulbecco's modified Eagle's medium (DMEM, Wako Pure Chemical Industries, Japan) containing 10% fetal bovine serum (FBS), 100 units/mL penicillin, 100 μg/mL streptomycin, and 0.25 μg/mL amphotericin B. The cells were incubated in 5% CO_2 at 37 °C.

Cellular Uptake of ANPs. The uptake of ANPs by RAW264.7 was observed by CLSM and analyzed using flow cytometry. The RAW264.7 cells (1 × 10^6) after trypsinization were incubated with ANPs (50 μg/mL, aspect ratio 10 (AR10)) in PBS for 1 h at 37 °C. After the centrifugation, the cells were washed with PBS and fixed with a 10% formalin solution. The cells were placed on a coverslip and observed by CLSM (Fv10i, Olympus, Japan). The cell-associated fluorescence was measured by flow cytometry (Cell Sorter SH800, Sony, Japan).

Cytocompatibility and Enzyme-Linked Immunosorbent Assay (ELISA). The cytocompatibility of ANPs and the secretion of tumor necrosis factor-α (TNF-α) from macrophage-like cells exposed to ANPs were measured using a lactate dehydrogenase (LDH) assay kit (Cayman Chemical) and ELISA assay (Thermo Fisher Scientific). Then, 2.5 × 10^4 RAW264.7 cells were seeded onto a 48-well plate and cultured in DMEM for 24 h. The culture medium

https://dx.doi.org/10.1021/acs.biomac.9b01775
Biomacromolecules 2020, 21, 2043−2048

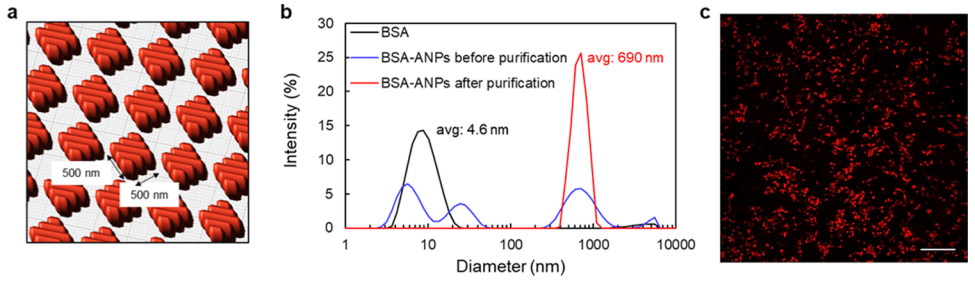

Figure 2. (a) Design of an array of cuboid particles (500 nm × 500 nm × 240 nm). (b) DLS measurement of the mixture of BSA and BSA ANPs before and after purification by dialysis and freeze-drying. (c) CLSM image of ANPs labeled with RB. Scale bar, 20 μm.

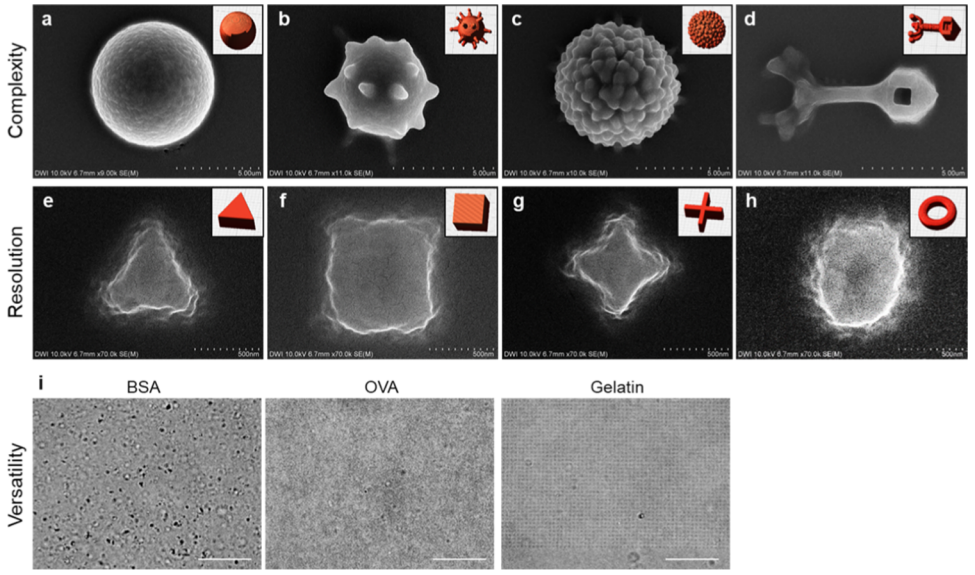

Figure 3. (a–h) Design and SEM images of ANPs with distinct morphologies: (a) sphere, (b, c) particle with a spiky projection, (d) virus-like structure, (e) triangle, (f) square, (g) cross, and (h) ring shape. (i) Phase-contrast images of ANPs composed of 10 wt % BSA, OVA, and gelatin and 5 mM RB. A laser intensity of 100 mW and scanning speeds of 2000 μm/s for BSA and gelatin and 400 μm/s for OVA were used. Scale bars, 20 μm.

was then replaced by a medium containing a mixture of BSA and OVA (9:1 (w/w), 50 μg/mL) and ANPs with AR1, AR3, and AR10. After 24 h of incubation at 37 °C, the supernatant was collected from each well and LDH and ELISA assays were performed according to the manufacturer's procedures.

Statistical Analysis. All data were expressed as means ± standard deviation (SD) from three independent experiments unless otherwise specified. Statistical differences from ELISA analyses were determined by one-way analysis of variance (ANOVA) with the Tukey–Kramer method. A p value less than 0.05 was considered to be statistically significant.

RESULTS AND DISCUSSION

Preparation of ANPs by MPL. For 3D-printing of ANPs by MPL, a photoresist composed of an antigen and a photosensitizer was chemically cross-linked by radical formation on amino acids containing an aromatic group through the two-photon excitation of the photosensitizer. Through this reaction, ANPs were formed in the focal volume of a laser beam, which was substantially confined due to the nonlinear optical process. The lateral and axial radii of the focal point are estimated as 150 and 240 nm, respectively[26] (numerical aperture: 1.4, refractive index of photoresist, n: 1.41,[27] wavelength of light: 780 nm), which determines the resolution of 3D-printing. As a model protein, bovine serum albumin (BSA), which is well known as an experimental model antigen, was employed. The 40 wt % BSA and 5 mM RB as a photosensitizer were dissolved in PBS. The protein photoresist on a coverslip was placed on the stage of MPL with a pulsed femtosecond laser, a 3D-piezo scanning stage, and an oil-immersion 63× objective lens. We started with the design and printing of an array of cuboid ANPs (Figure 2a). For the mass production of ANPs, the design of a cuboid was simplified and composed of five overlapped lines with a 100 nm hatching distance (500 nm × 500 nm × 240 nm in design). The printed ANPs were purified by dialysis and freeze-dried. DLS measurements showed that the size of ANPs was homogeneously distributed and the average diameter was 690 nm after the purification process, which was in good agreement with the original design (Figure 2b). These ANPs were stable after the freeze-drying process, which is important for storage, transport, and less contamination. Fourier transform infrared (FT-IR) spectroscopic measurements showed the presence of RB in ANPs because a small fraction of RB was linked to ANPs through a radical reaction during the particle formation (Figure S1). Therefore, the obtained ANPs can be visualized by fluorescence observations. CLSM displayed the successful preparation of BSA ANPs (Figure 2c). Moreover, the 3D-printing system of ANPs does not require any complicated processes including the use of toxic materials, encapsulation of antigens, and labeling for visualization.

https://dx.doi.org/10.1021/acs.biomac.9b01775
Biomacromolecules 2020, 21, 2043–2048

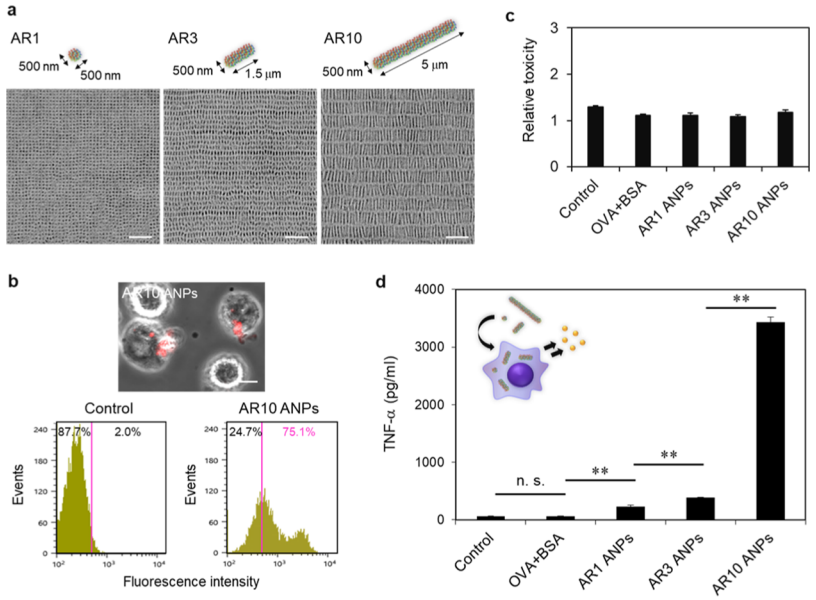

Figure 4. (a) Schematic illustration and phase-contrast images of ANPs with distinct ARs in the range of 1−10 (AR1: 500 nm × 500 nm × 500 nm, AR3: 500 nm × 500 nm × 1.5 μm, AR10: 500 nm × 500 nm × 5 μm). (b) CLSM image and flow cytometry analysis of uptake of ANPs (100 mg/mL, AR10) by RAW264.7 after 1 h of incubation. (c) LDH assay of control (without antigen), as-prepared antigens (50 mg/mL), and ANPs (with AR1, AR3, and AR10). The values of LDH were standardized by that of DMEM. There were no significant differences (n = 3). (d) ELISA assay of TNF-α secreted from RAW264.7 when exposed to as-prepared antigens (50 μg/mL) and ANPs (with AR1, AR3, and AR10) for 24 h. $^{**}P < 0.01$ when compared with the control (Tukey−Kramer method, n = 3). The n.s. denotes no significant difference. Scale bars, 10 μm.

3D-Printing of Complex Nanostructures. The 3D-printing system by MPL allows for the rational design and precise control of the geometry of particles. To achieve morphological control of ANPs over a micro/nanoscale, we addressed the preparation of virus-like microparticles with nanoscale topological complexity. SEM images show a sphere 5 μm in diameter with a smooth surface and sub-microscale spiky projections and a virus-like structure (Figure 3a−d). Furthermore, to confirm the resolution of this system, we designed 500 nm diameter ANPs with different morphologies: triangular, square, crossed, and ring-shaped ANPs (Figure 3e−h). The resolution of the structure is more than 200−250 nm, which corresponds to the theoretical lateral and axial radii of the focal point (150 and 240 nm, respectively). These results suggest that the MPL-based 3D-printing approach is suitable to fabricate shape-designed micro/nanometer-sized ANPs with topological complexity that mimics the morphologies of bacteria and viruses in nature. As in nature, the complex shape of the viruses enables them to efficiently infect the host, this technique, which can precisely prepare a virus-like structure, would be of great advantage for a novel vaccine system to elicit immune responses with higher efficiency and lower toxicity than the conventional vaccines. Since this method is based on cross-linking of amino acids in proteins, a variety of proteins can be applied to fabricate ANPs. OVA and gelatin were used as model proteins. The photoresist of BSA was efficiently cross-linked, while that of OVA formed few ANPs due to the intrinsic properties of proteins including the molecular weight, solubility, viscosity, and sequence of amino acids (Figure 3i). On the other hand, the gelatin photoresist easily formed protein particles because, during the particle formation, gelation occurred at room temperature and the viscosity was increased, which facilitated the cross-linking. This result highlights the versatility of this method for a vaccine system. Based on this result, a mixture of BSA and OVA (9:1 (w/w)) was used for the following experiments since BSA shows an efficient cross-linking reaction and OVA is a well-known antigen model. The obtained BSA−OVA ANPs were also monodisperse after the purification (Figure S2).

Induction of Immune Responses by 3D-Designed ANPs. To evaluate the ability of 3D-printed ANPs and the effect of their shape on immune responses, we printed cuboid-shaped ANPs with distinct ARs in a range of 1−10 (AR1: 500 nm × 500 nm × 500 nm, AR3: 500 nm × 500 nm × 1.5 μm, AR10: 500 nm × 500 nm × 5 μm) (Figure 4a). First, the uptake behavior of ANPs by APCs was evaluated. The AR10 ANPs were incubated with macrophage-like RAW264.7 cells for 1 h. CLSM observation and flow cytometry analysis show that when RAW264.7 cells were exposed to AR10 ANPs, cell population above the threshold was 75.1%, which demonstrated that AR10 NPs were efficiently taken up by immune cells (Figure 4b). The cytocompatibility of ANPs was evaluated by the leakage of LDH, which is an intracellular enzyme and is leaked when the cell membrane is damaged. From the results obtained, all ARs of 3D-printed ANPs might be cytocompatible at 50 μg/mL (Figure 4c). Finally, we addressed the induction of immune responses using ANPs by measuring the secretion of TNF-α. When the APCs are stimulated by pathogens, they secrete many proinflammatory cytokines such as TNF-α and interleukins and initiate immune reactions.[28] We found that the secretion of TNF-α substantially increased using 3D-printed ANPs (more than 4-fold increase), while as-prepared proteins showed no immune induction compared to the control (Figure 4d). These results indicate that ANPs have the ability to enhance the immune response. While small soluble antigens showed little uptake by APCs at 50 μg/mL, micrometer-sized particulate antigens may be taken up efficiently through the endocytosis pathway.[17] Furthermore, a higher AR of ANPs induced higher secretion of TNF-α. Surprisingly, AR10 ANPs showed a 58-fold increase of

https://dx.doi.org/10.1021/acs.biomac.9b01775
Biomacromolecules 2020, 21, 2043−2048

the secretion of TNF-α, even though the number of AR1 ANPs was 10 times as much as that of AR10 ANPs theoretically, suggesting strong shape-dependent immune induction. Compared to spherical particles, the high AR of long ANPs might show higher adhesion probability and disruption of the cell membrane due to tumbling and larger contact area with cell membranes.[16,18,29,30] Thus, this MPL-based 3D-printing system of ANPs may serve as a new platform to fabricate 3D-shape-designed antigen particles.

We summarized the comparison of 3D-printed ANPs to other protein particle systems (Table S1). Self-assembled antigen particles have the advantages of nanoscale fabrication, dispersity, and cytocompatibility, while these lack versatility in protein type due to the need for specific physical interactions like hydrophobic and electrostatic interactions to form a particle. The chemical cross-linking of antigens might be a versatile fabrication method. However, toxic cross-linkers such as dithiothreitol may remain in particles and substantially impair the protein activity. Spray-freeze-drying processes, though highly versatile, cytocompatible, and active, they have limitations in nanoscale fabrication and dispersity. None of the conventional methods can design the geometry of antigen particles. Although the molding method allows for geometrical control, it is limited only to the fabrication of 2D structures. We show that the MPL-based 3D-printing approach produces monodisperse, versatile, and cytocompatible antigen particles with a geometric design on a nanoscale. For further development of this system, nanoparticle designs that can induce endosome escape need to be elucidated for enhancing the efficacy of antigen delivery. In terms of denaturation of antigens after MPL, radical reactions might cause denaturation. However, the antigens, after cellular uptake, are degraded to peptides in the endosome and only several amino acid sequences are required for immune induction.[31] Therefore, the effect of denaturation of antigens could be a negligible problem for vaccine systems. This method has enormous potential to overcome these limitations toward a novel vaccine delivery system.

CONCLUSIONS

In conclusion, we developed a carrier-free and 3D-shape-designed ANP by an MPL-based 3D-printing approach. This 3D-lithographic approach provides freedom for the precise design of particle shapes with a nanoscale resolution. The obtained ANPs displayed high complexity of micro/nanoscale features and versatility for protein types including BSA, OVA, and gelatin. The ANPs with distinct ARs showed uptake by macrophage-like cells, and LDH assays suggested that ANPs were cytocompatible. Importantly, the ANPs enhanced the secretion of TNF-α and the higher AR of particles substantially amplified the secretion. The 3D-printing approach for the rational design of nanomaterials with increasing safety, complexity, and efficacy has enormous potential to develop an efficient drug-delivery carrier for vaccine delivery and may offer a mechanistic understanding of structure−function relationships.

ASSOCIATED CONTENT

Supporting Information

The Supporting Information is available free of charge at https://pubs.acs.org/doi/10.1021/acs.biomac.9b01775.

FT-IR measurement and DLS measurement of nanoparticles; Fourier transform infrared spectroscopy (FT-IR) spectra of BSA, RB, and BSA ANPs; DLS measurement of BSA−OVA ANPs in PBS after freeze-drying; comparison of 3D-printed ANPs to other protein particle systems (PDF)

AUTHOR INFORMATION

Corresponding Author

Martin Moeller − *DWI—Leibniz-Institute for Interactive Materials, RWTH Aachen University, D-52056 Aachen, Germany;* orcid.org/0000-0002-5955-4185; Email: moeller@dwi.rwth-aachen.de

Authors

Akihiro Nishiguchi − *DWI—Leibniz-Institute for Interactive Materials, RWTH Aachen University, D-52056 Aachen, Germany;* orcid.org/0000-0002-3160-6385

Fumiaki Shima − *Graduate School of Frontier Biosciences, Osaka University, Suita 565-0871, Osaka, Japan*

Smriti Singh − *DWI—Leibniz-Institute for Interactive Materials, RWTH Aachen University, D-52056 Aachen, Germany;* orcid.org/0000-0002-2164-9912

Mitsuru Akashi − *Graduate School of Frontier Biosciences, Osaka University, Suita 565-0871, Osaka, Japan*

Complete contact information is available at: https://pubs.acs.org/10.1021/acs.biomac.9b01775

Notes

The authors declare no competing financial interest.

ACKNOWLEDGMENTS

This work was supported by SFB 985-Functional Microgels and Microgel Synthesis, the ERC Advanced Grant 695716, and the Center for Chemical Polymer Technology supported by the EU and the state of North Rhine-Westphalia (Grant no. EFRE 30 00 883 02).

REFERENCES

(1) Hubbell, J. A.; Thomas, S. N.; Swartz, M. A. Materials engineering for immunomodulation. *Nature* **2009**, *462*, 449−460.

(2) Moon, J. J.; Huang, B.; Irvine, D. J. Engineering nano- and microparticles to tune immunity. *Adv. Mater.* **2012**, *24*, 3724−3746.

(3) Bachmann, M. F.; Jennings, G. T. Vaccine delivery: a matter of size, geometry, kinetics and molecular patterns. *Nat. Rev. Immunol.* **2010**, *10*, 787−796.

(4) Foged, C.; Sundblad, A.; Hovgaard, L. Targeting vaccines to dendritic cells. *Pharm. Res.* **2002**, *19*, 229−238.

(5) Banchereau, J.; Steinman, R. M. Dendritic cells and the control of immunity. *Nature* **1998**, *392*, 245−252.

(6) Jiang, W.; Gupta, R. K.; Deshpande, M. C.; Schwendeman, S. P. Biodegradable poly(lactic-co-glycolic acid) microparticles for injectable delivery of vaccine antigens. *Adv. Drug Delivery Rev.* **2005**, *57*, 391−410.

(7) Shima, F.; Akagi, T.; Uto, T.; Akashi, M. Manipulating the antigen-specific immune response by the hydrophobicity of amphiphilic poly(γ-glutamic acid) nanoparticles. *Biomaterials* **2013**, *34*, 9709−9716.

(8) Geng, Y.; Dalhaimer, P.; Cai, S.; Tsai, R.; Tewari, M.; Minko, T.; Discher, D. E. Shape effects of filaments versus spherical particles in flow and drug delivery. *Nat. Nanotechnol.* **2007**, *2*, 249−255.

(9) Murthy, N.; Xu, M.; Schuck, S.; Kunisawa, J.; Shastri, N.; Fre′chet, J. M. J. *Proc. Natl. Acad. Sci. U.S.A.* **2003**, *100*, 4995.

(10) O'Hagan, D. T.; Valiante, N. M. Recent advances in the discovery and delivery of vaccine adjuvants. *Nat. Rev. Drug Discovery* **2003**, *2*, 727−735.
(11) Volodkin, D. V.; Schmidt, S.; Fernandes, P.; Larionova, N. I.; Sukhorukov, G. B.; Duschl, C.; Möhwald, H.; von Klitzing, R. One-step formulation of protein microparticles with tailored properties: hard templating at soft conditions. *Adv. Funct. Mater.* **2012**, *22*, 1914−1922.
(12) Chiu, Y. C.; Gammon, J. M.; Andorko, J. M.; Tostanoski, L. H.; Jewell, C. M. Modular vaccine design using carrier-free capsules assembled from polyionic immune signals. *ACS Biomater. Sci. Eng.* **2015**, *1*, 1200−1205.
(13) Kelly, J. Y.; DeSimone, J. M. Shape-specific, monodisperse nano-molding of protein particles. *J. Am. Chem. Soc.* **2008**, *130*, 5438−5439.
(14) Wang, Z. L.; Finlay, W. H.; Peppler, M. S.; Sweeney, L. G. Powder formation by atmospheric spray-freeze-drying. *Powder Technol.* **2006**, *170*, 45−52.
(15) Chen, Q.; Liu, X.; Chen, J.; Zeng, J.; Cheng, Z.; Liu, Z. A self-assembled albumin-based nanoprobe for in vivo ratiometric photoacoustic pH imaging. *Adv. Mater.* **2015**, *27*, 6820−6827.
(16) Mitragotri, S.; Lahann, J. Physical approaches to biomaterial design. *Nat. Mater.* **2009**, *8*, 15−23.
(17) Akagi, T.; Shima, F.; Akashi, M. Intracellular degradation and distribution of protein-encapsulated amphiphilic poly(amino acid) nanoparticles. *Biomaterials* **2011**, *32*, 4959−4967.
(18) Alexis, F.; Pridgen, E.; Molnar, L. K.; Farokhzad, O. C. Factors affecting the clearance and biodistribution of polymeric nanoparticles. *Mol. Pharm.* **2008**, *5*, 505−515.
(19) Doshi, N.; Mitragotri, S. Macrophages recognize size and shape of their targets. *PLoS One* **2010**, *5*, No. e10051.
(20) Gratton, S. E. A.; Ropp, P. A.; Pohlhaus, P. D.; Luft, J. C.; Madden, V. J.; Napier, M. E.; DeSimone, J. M. The effect of particle design on cellular internalization pathways. *Proc. Natl. Acad. Sci. U.S.A.* **2008**, *105*, 11613−11618.
(21) Toy, R.; Peiris, P. M.; Ghaghada, K. B.; Karathanasis, E. Shaping cancer nanomedicine: the effect of particle shape on the in vivo journey of nanoparticles. *Nanomedicine* **2014**, *9*, 121−134.
(22) Zhang, Y. L.; Chen, Q. D.; Xia, H.; Sun, H. B. Designable 3D nanofabrication by femtosecond laser direct writing. *Nano Today* **2010**, *5*, 435−448.
(23) Maruo, S.; Nakamura, O.; Kawata, S. Three-dimensional microfabrication with two-photon-absorbed photopolymerization. *Opt. Lett.* **1997**, *22*, 132−134.
(24) Campagnola, P. J.; Delguidice, D. M.; Epling, G. A.; Hoffacker, K. D.; Howell, A. R.; Pitts, J. D.; Goodman, S. L. 3-dimensional submicron polymerization of acrylamide by multiphoton excitation of xanthene dyes. *Macromolecules* **2000**, *33*, 1511−1513.
(25) Kaehr, B.; Shear, J. B. Multiphoton fabrication of chemically responsive protein hydrogels for microactuation. *Proc. Natl. Acad. Sci. U.S.A.* **2008**, *105*, 8850−8854.
(26) Tibbitt, M. W.; Kloxin, A. M.; Dyamenahallic, K. U.; Anseth, K. S. Controlled two-photonphotodegradation of PEG hydrogels to study and manipulate subcellular interactions on soft materials. *Soft Matter* **2010**, *6*, 5100−5108.
(27) Barer, R.; Tkaczyk, S. Refractive index of concentrated protein solutions. *Nature* **1954**, *173*, 821−822.
(28) Yi, A. K.; Yoon, J. G.; Hong, S. C.; Redford, T. W.; Krieg, A. M. Lipopolysaccharide and CpG DNA synergize for tumor necrosis factor-alpha production through activation of NF-kappaB. *Int. Immunol.* **2001**, *13*, 1391−1404.
(29) Decuzzi, P.; Ferrari, M. The adhesive strength of non-spherical particles mediated by specific interactions. *Biomaterials* **2006**, *27*, 5307−5314.
(30) Doshi, N.; Mitragotri, S. Needle-shaped polymeric particles induce transient disruption of cell membranes. *J. R. Soc., Interface* **2010**, *7*, S403−S410.
(31) Neefjes, J.; Jongsma, M. L. M.; Paul, P.; Bakke, O. Towards a systems understanding of MHC class I and MHC class II antigen presentation. *Nat. Rev. Immunol.* **2011**, *11*, 823−836.

https://dx.doi.org/10.1021/acs.biomac.9b01775
Biomacromolecules 2020, 21, 2043−2048